Electronic Supplementary Information

Plasmonic hot charge carriers activated Ni centres of metal-organic frameworks for oxygen evolution reaction

Wen-Chao Hu,[a,b] Yi Shi,[a] Yue Zhou,[a] Chao Wang,[c] Muhammad Rizwan Younis,[a] Jie Pang,[a] Chen Wang,[*b] Xing-Hua Xia[*a]

Water splitting for oxygen evolution reaction (OER) through electrocatalysis holds a significant promise for energy conversion. However, its real application is yet hindered owing to the lack of efficient electrocatalysts. Herein, we propose a plasmon activation approach to the acceleration of OER on an Au nanorods-2D ultrathin metal-organic frameworks (NiCo-MOFs) hybrid. The plasmon generated hot holes of Au nanorods (AuNRs) can be injected into the nickel active sites of the OER catalysts, significantly increasing the generation of high valence Ni* active species in NiCo-MOFs with better matched energy level for OER, in turn decreasing the OER activation energy. Thus, excellent OER performance of the NiCo-MOFs under surface plasmon resonance of AuNRs is achieved with an overpotential of 240 mV at the current density of 10 mA cm^{-2} and a Tafel slope of 69 mV dec^{-1}, which is much better than the now-a-days reported catalysts. This finding highlights the importance of noble metal LSPR in facilitating OER performance of MOFs and opens up a new avenue for improving the intrinsic electrocatalytic activity of pristine MOFs.

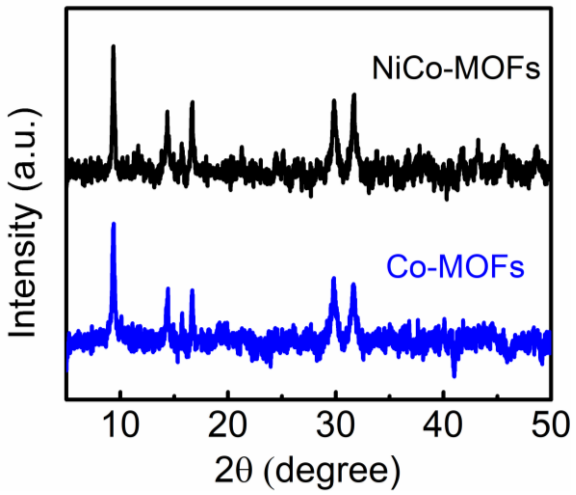

Figure S1. XRD pattern of NiCo-MOFs and Co-MOFs.

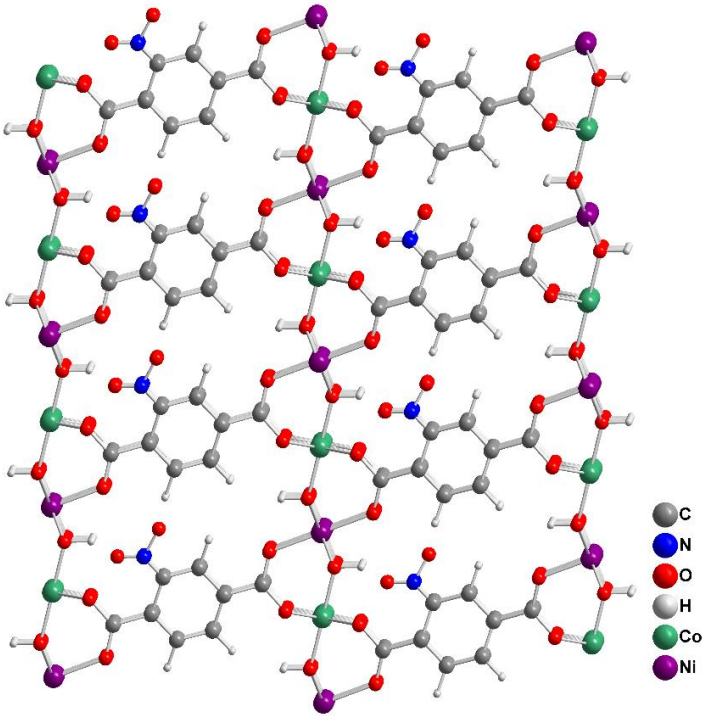

Figure S2. Atomic arrangement of NiCo-MOFs.

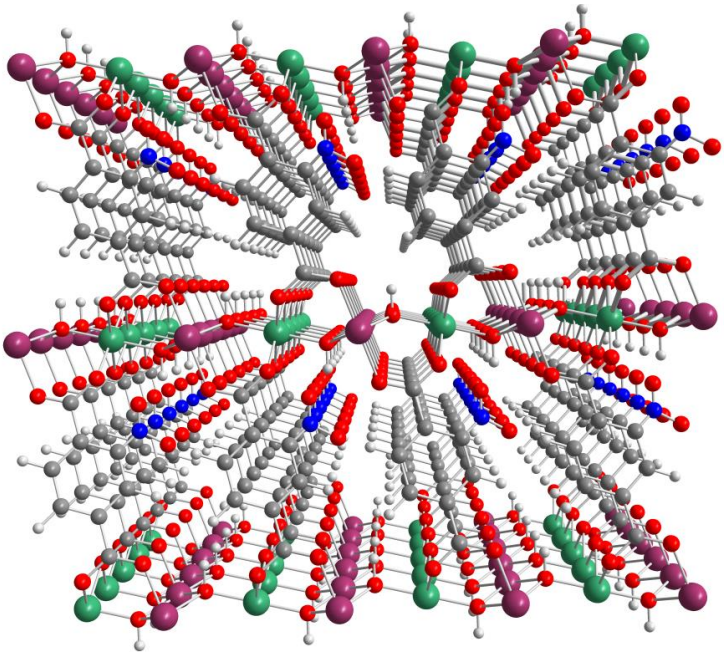

Figure S3. Crystal structure of NiCo-MOFs.

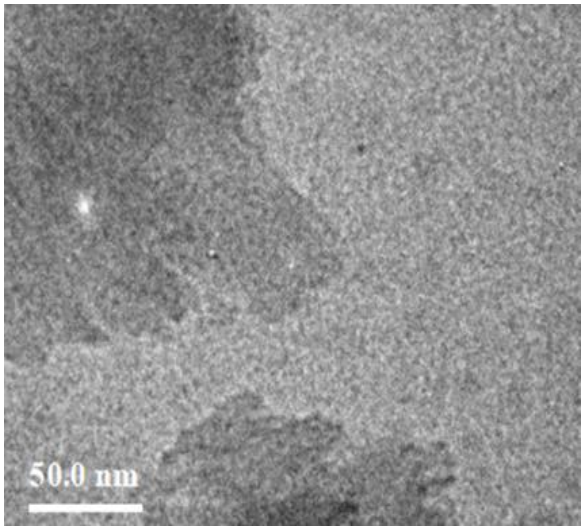

Figure S4. TEM image of NiCo-MOFs after 2.0 h OER performance showing that the 2D layered structure of NiCo-MOFs is maintained.

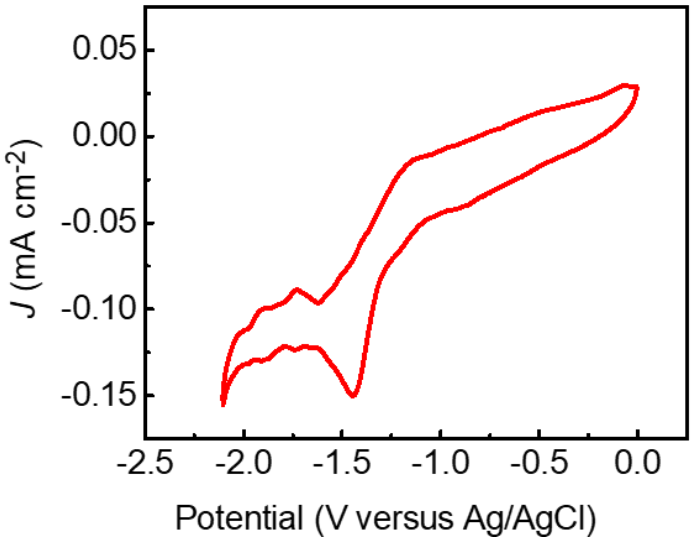

Figure S5. Cyclic voltammogram of NiCo-MOFs in a solution of 0.1 M CH_3CN under N_2 atmosphere at a scan rate of 30 mV/s. The LUMO energy levels is calculated from the onset reduction potential (E_{red}) using the following equation: $E_{LUMO} = -(E_{red} + 4.71)$ eV. The onset reduction potential is located at -1.30 V versus the Ag/AgCl reference electrode. The E_{LUMO} is then calculated as -3.41 eV *vs* Vacuum level and ϕ_{LUMO} is as -[-3.41-(-4.5)] = -1.09 V *vs* NHE.[1]

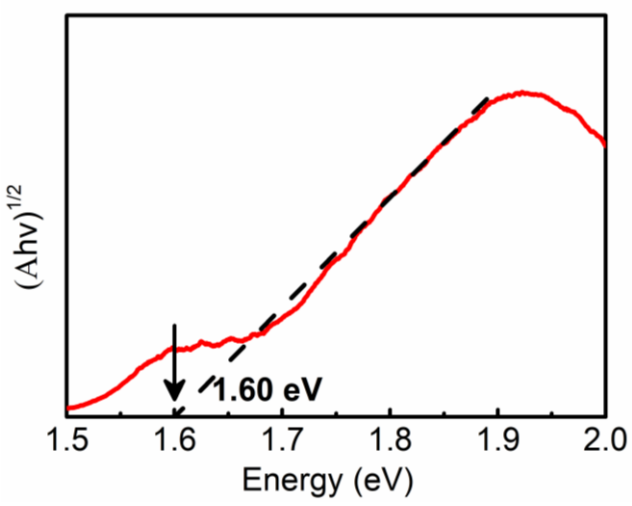

Figure S6. The band gap of NiCo-MOFs is determined to be 1.60 eV by extrapolating the linear region of the absorbance spectrum subduplicate.

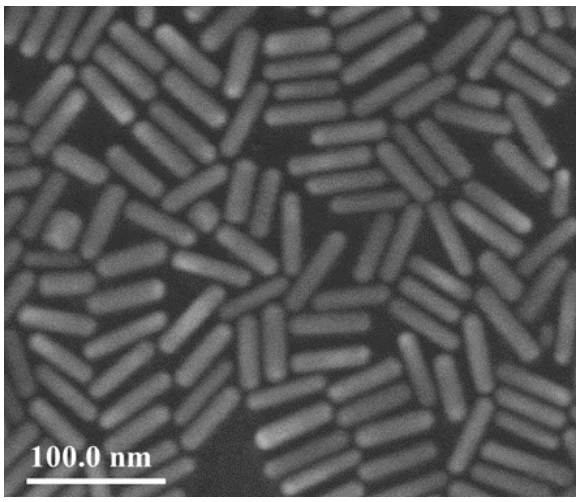

Figure S7. SEM image of Au nanorods.

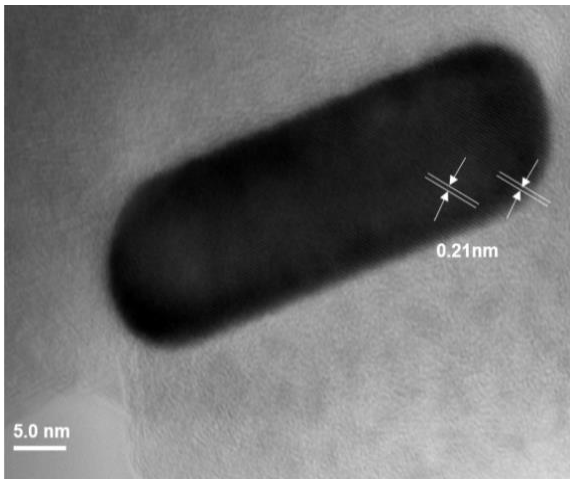

Figure S8. HR-TEM images of AuNRs/NiCo-MOFs hybrid.

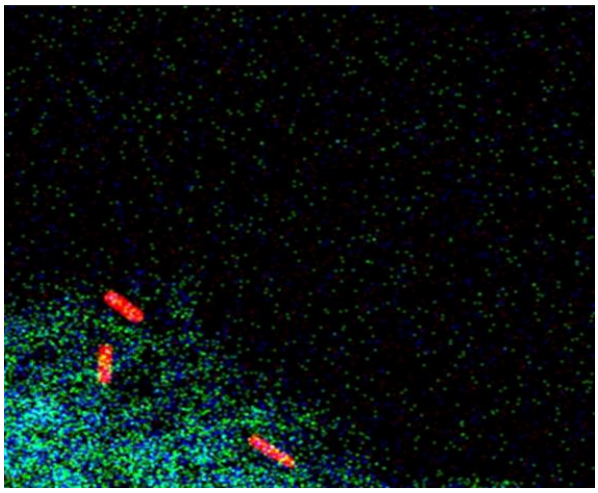

Figure S9. Element mapping image of Au (red), Ni (blue) and Co (yellow) in AuNRs/NiCo-MOFs.

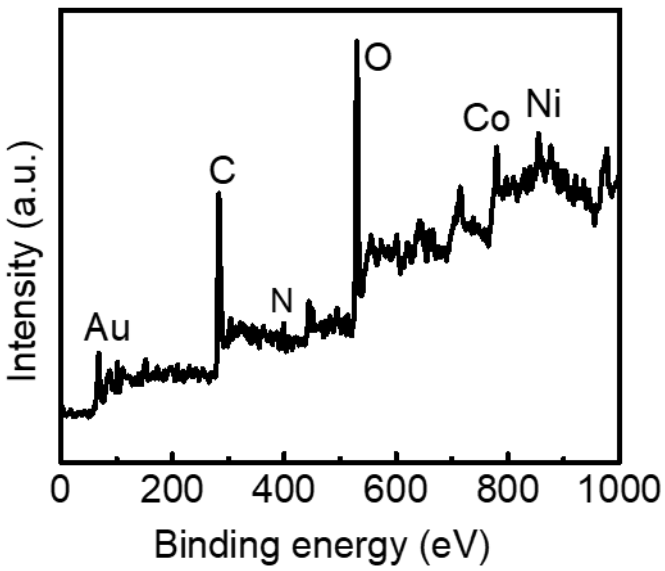

Figure S10. XPS survey spectrum of AuNRs/NiCo-MOFs.

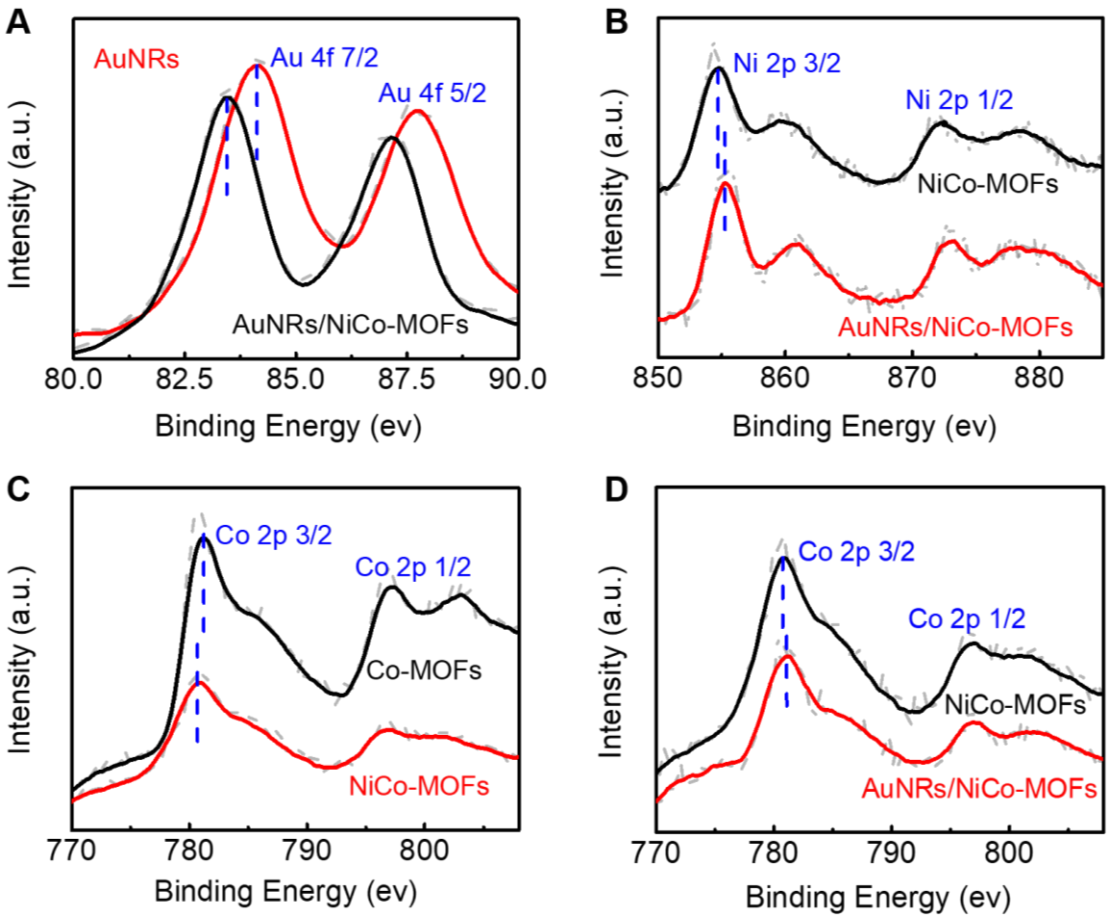

Figure S11. High-resolution XPS spectra of AuNRs, NiCo-MOFs, Co-MOFs and AuNRs/NiCo-MOFs of Au 4f (A), Ni 2p (B), Co 2p (C) and (D).

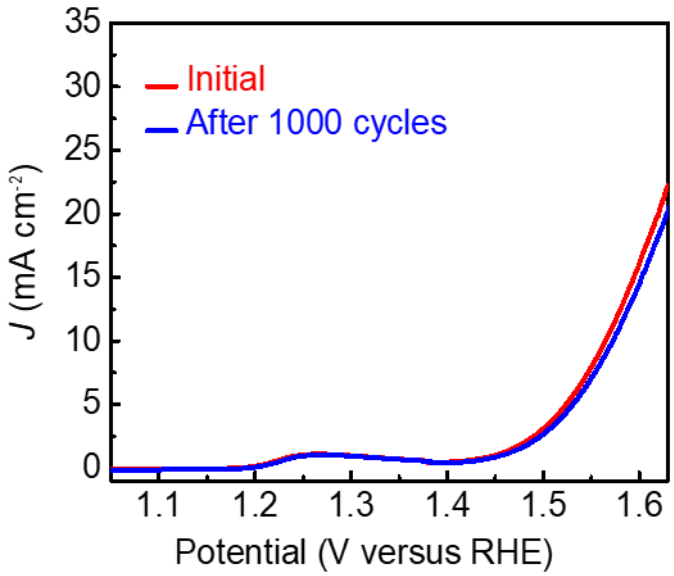

Figure S12. Stability tests of NiCo-MOFs before and after 1000 cyclic potential scans in 1.0 M KOH.

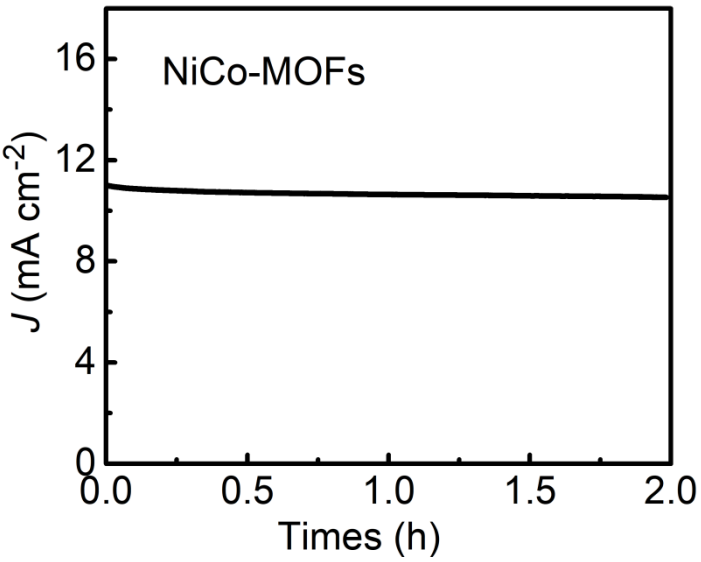

Figure S13. Chronoamperometric *J-t* curve of NiCo-MOFs in 1.0 M KOH at 1.57 V (versus RHE) for 2.0 h.

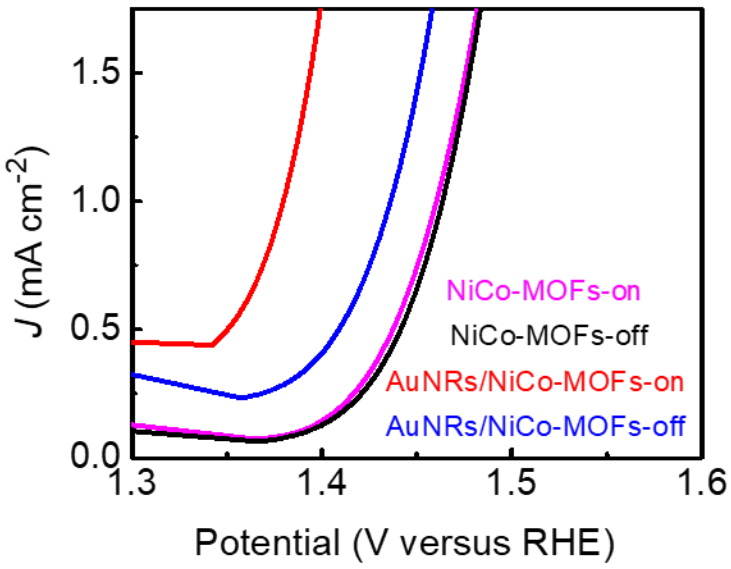

Figure S14. Magnified LSV curves of AuNRs/NiCo-MOFs-on, AuNRs/NiCo-MOFs-off, NiCo-MOFs-on and NiCo-MOFs-off in a solution of 1.0 M KOH at a scan rate of 10 mV s^{-1}.

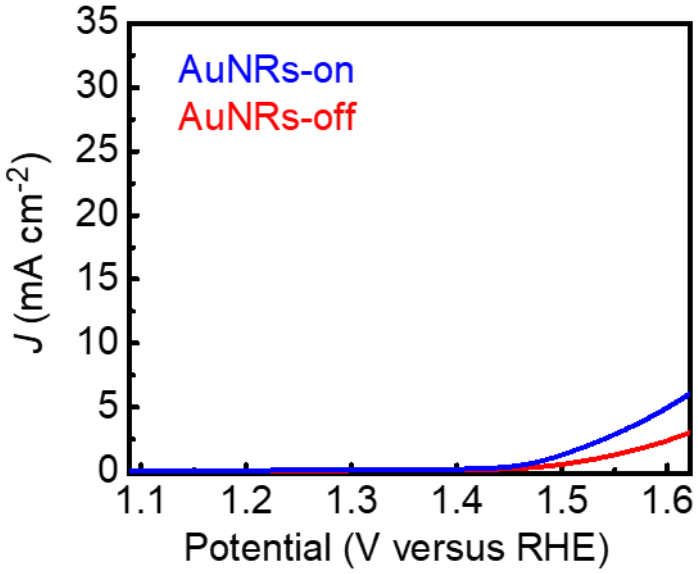

Figure S15. OER activity of AuNRs in a solution of 1.0 M KOH with light irradiation on and off. Scan rate was 10 mV s^{-1}.

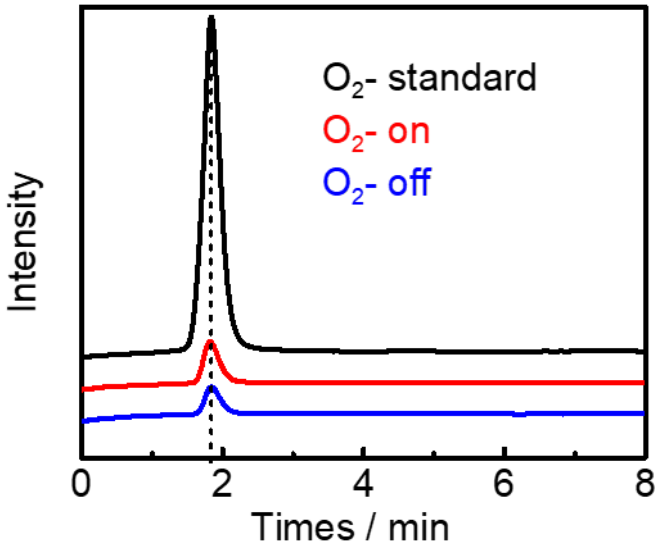

Figure S16. Gas chromatography (GC) measurement of products in different samples. O_2-standard: collected from the gas cylinder; O_2-on: gas collected from the working electrode under 808 nm laser irradiation; O_2-off: gas collected from the working electrode with laser off. The N_2 was purged for 1.5 h before each continuous gas-collecting operation. The electrolyte in a solution of 1.0 M KOH was performed at an overpotential of 0.22 V.

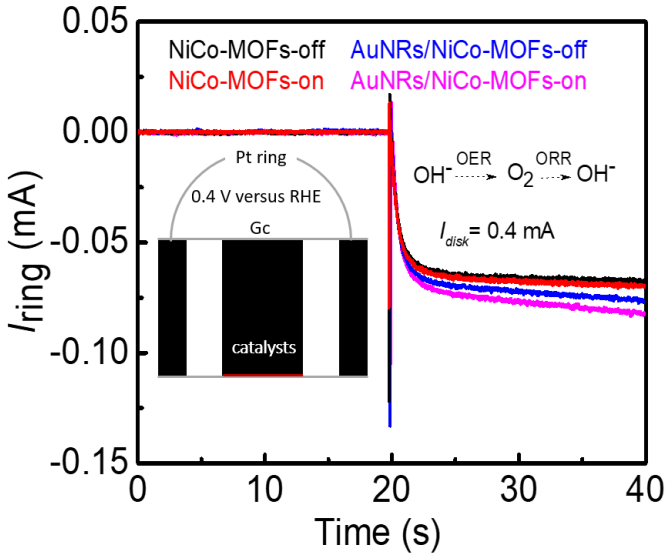

Figure S17. Faradaic efficiency testing of the different samples using rotating ring disk electrode (RRDE) in N_2-saturated 1.0 M KOH solution at a rotation speed of 1600 rpm. The O_2 generated on GCE disk will be reduced on the Pt ring electrode biased at 0.4 V *vs* RHE. The Faradaic efficiency (FE) is calculated using the previous methods: [2]

$$\mathrm{FE} = \frac{I_{ring}}{C_e \times I_{disk}} \qquad \text{(S-1)}$$

I_{disk} is the current collected on the disk electrode. I_{ring} is the current collected on the Pt ring electrode, C_e (~0.2) is the oxygen collection coefficient.[2]

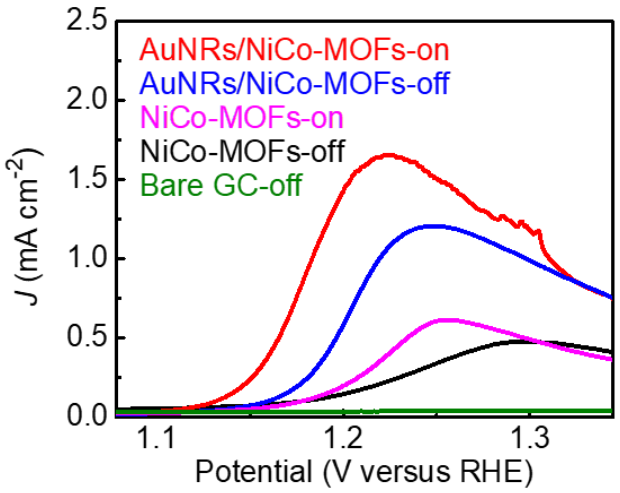

Figure S18. Magnified LSV curve of AuNRs/NiCo-MOFs and NiCo-MOFs in a solution of 1.0 M KOH at scan rate of 10 mV s^{-1}. The anodic wave in the potential range from 1.15 V to 1.30 V could be ascribed to the oxidation of Ni.

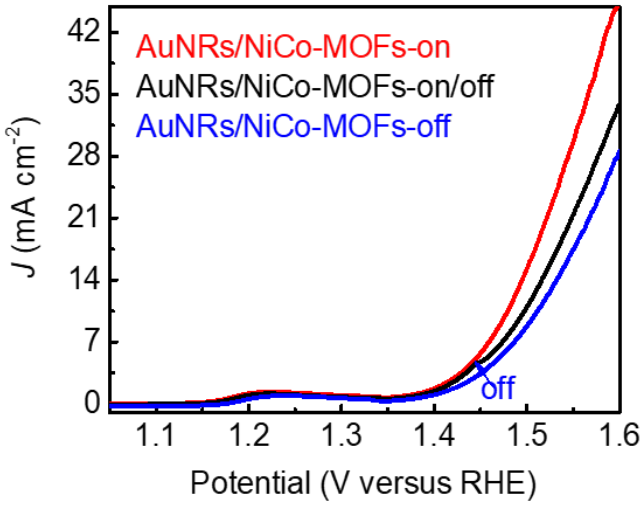

Figure S19. LSV curves of AuNRs/NiCo-MOFs in a solution of 1.0 M KOH with 808 nm light irradiation on and off. The scan rate was 10 mV s^{-1}.

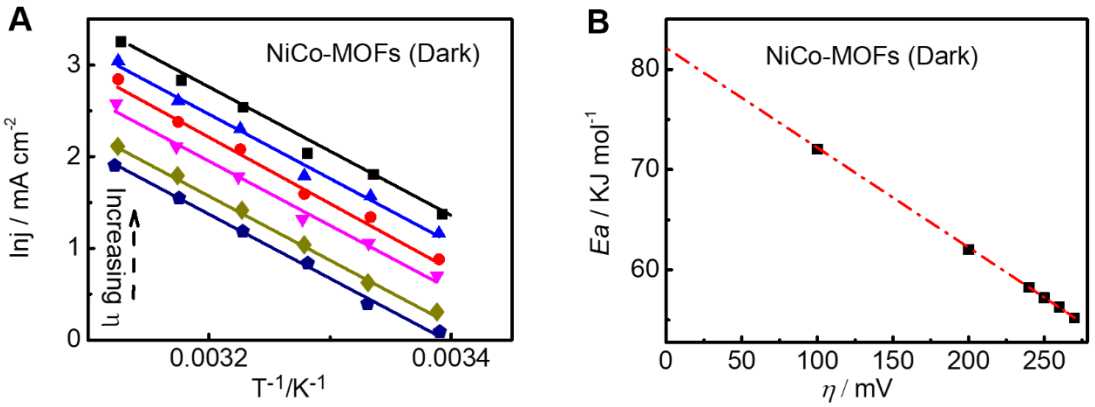

Figure S20. Arrhenius plots: semi-logarithmic dependence of current density of the NiCo-MOFs at various overpotentials plotted against inverse temperature. Overpotentials are taken from 100 to 270 mV under light off (A). Activation energy at the zero overpotential obtained through trend extrapolation of NiCo-MOFs (B).

The OER activation energy of NiCo-MOFs and AuNRs/NiCo-MOFs is estimated by using the Arrhenius equation and kinetic data. Plot of ln(*J*) as a function of the reciprocal of temperature (1/T) results in linear curves. The Arrhenius equation given in the form:

$$j = Ae^{-Ea/RT} \qquad \text{(S-2)}$$

Ea denotes the activation energy; A is the pre-exponential factor; T is the temperature (Kelvin) and R denotes the gas constant.

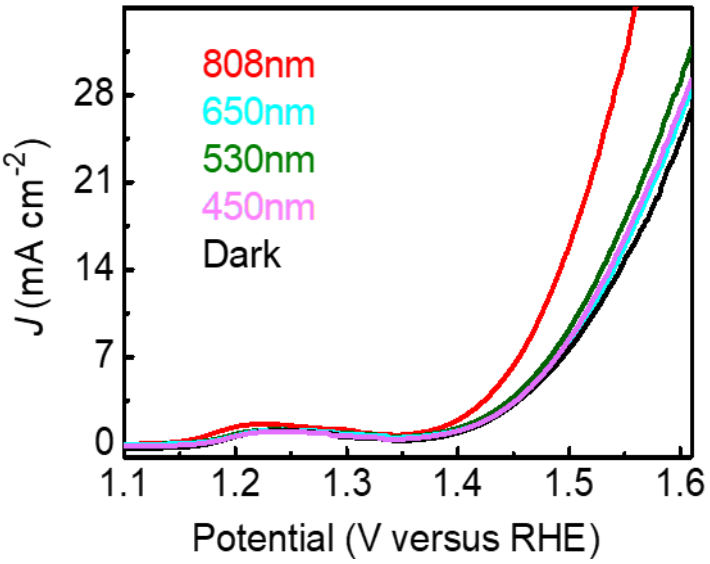

Figure S21. OER activity of the AuNRs/NiCo-MOFs hybrid under laser irradiation with different wavelength.

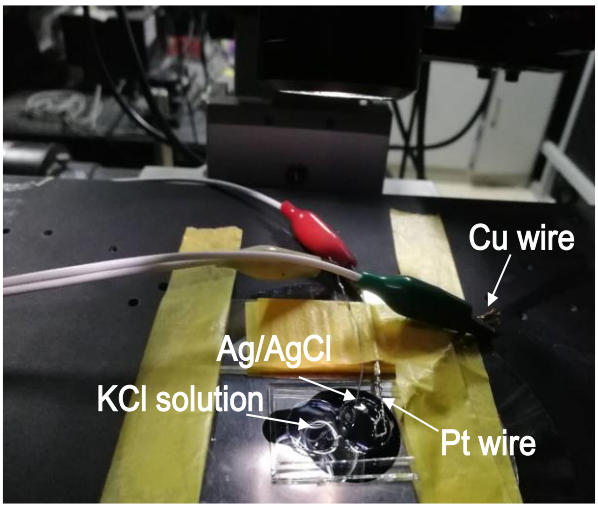

Figure S22. Dark-field electrochemical apparatus. Dark field images were acquired on a Nikon inverted microscope Eclipse Ti-U equipped with a colored CCD (Nikon, DS-FI1-U2). The local surface plasmon resonance (LSPR) scattering spectra were recorded using a SP2556 spectrograph mounted on the microscope, and a 512B excelon EMCCD was used as the detector (Princeton Instruments, USA).

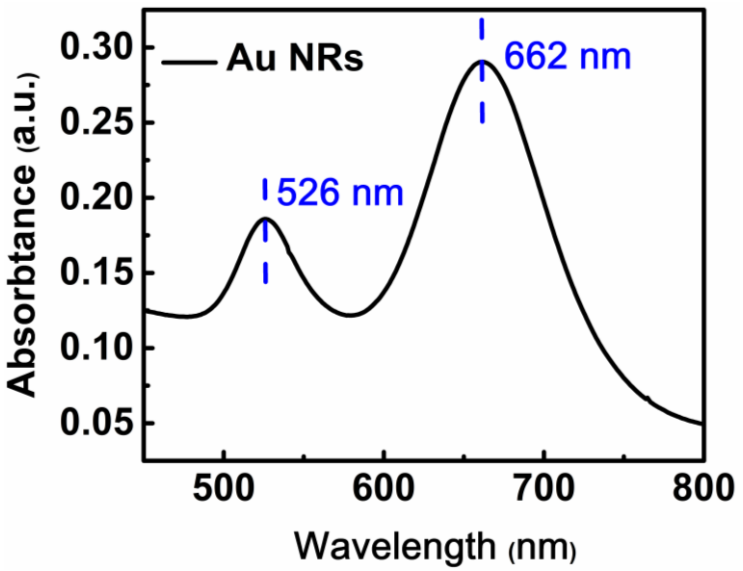

Figure S23. UV-vis spectrum of Au nanorods with LSPR longitudinal band centered at ~662 nm.

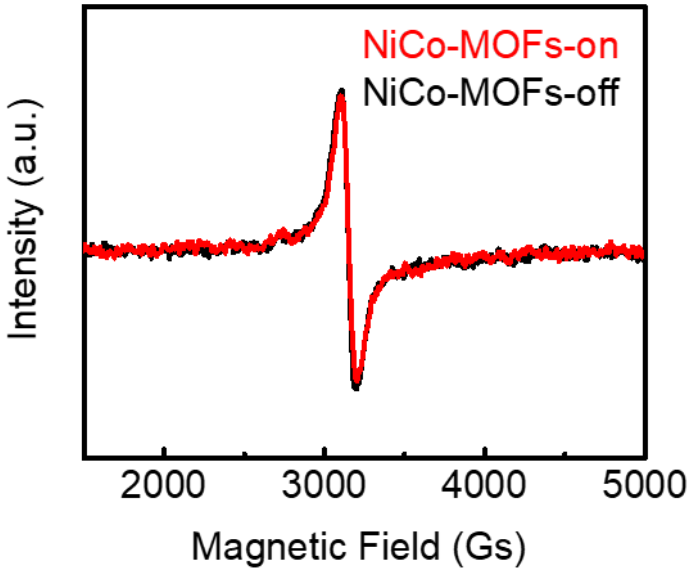

Figure S24. EPR spectra of NiCo-MOFs with light on and off.

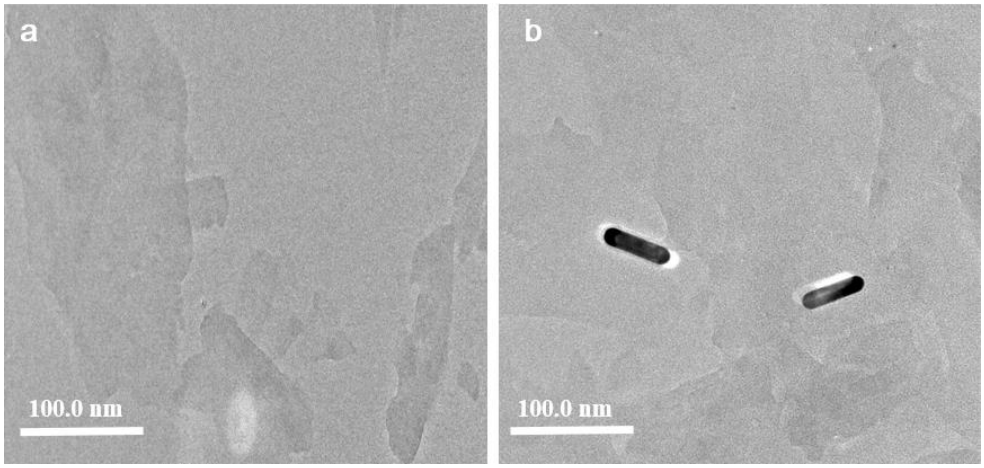

Figure S25. TEM images of Co-MOFs and AuNRs/Co-MOFs. a) Co-MOFs; b) AuNRs/Co-MOFs. The images clearly exhibit the 2D ultrathin layered structure.

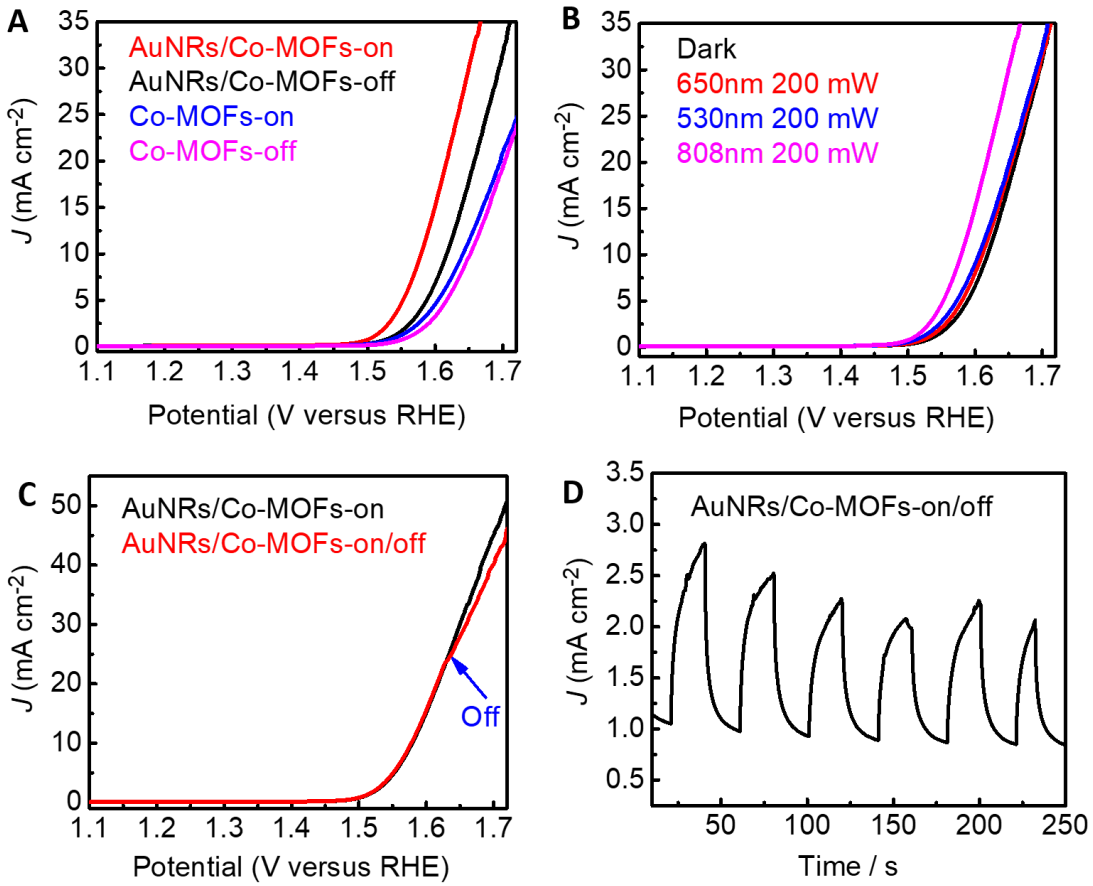

Figure S26. a) OER polarization curves of the AuNRs/Co-MOFs hybrid and Co-MOFs with laser (808 nm) on or off at a scan rate of 10 mV s^{-1}. b) OER activity of the AuNRs/Co-MOFs with different wavelength irradiation; the scan rate was 10 mV s^{-1}. c) Polarization curve of the AuNRs/Co-MOFs with 808 nm laser irradiation on and off; the scan rate was 10 mV s^{-1}. d) Chronoamperometric *J-t* curve of the AuNRs/Co-MOFs and Co-MOFs at 1.53 V under 808 nm laser illumination on and off. The electrolyte was 1.0 M KOH.

Table. S1 Comparison of OER activity of AuNRs/NiCo-MOFs and different active materials in 1.0 M KOH solution.

Samples	Onset Potential (V)	Overpotential @ 10 mA cm^{-2} (mV)	Substrate	Reference
AuNRs/NiCo-MOF (Light)	1.38	240	GCE	This work
AuNRs/NiCo-MOFs (Dark)	1.43	283	GCE	This work
NiCo-MOFs (Light)	1.46	335	GCE	This work
NiCo-MOFs (Dark)	1.46	345	GCE	This work
AuNRs/Co-MOFs(Light)	1.50	349	GCE	This work
AuNRs/Co-MOFs(Dark)	1.53	388	GCE	This work
Co-MOFs (Light)	1.55	401	GCE	This work
Co-MOFs (Dark)	1.56	421	GCE	This work
NiCo-UMOFNs	1.42	250	GCE	3
Co-UMOFNs	1.53	371	GCE	3
Ni-UMOFNs	1.46	321	GCE	3
NiFe-UMNs	1.45	260	GCE	4
CoFe-UMNs	1.52	350	GCE	4
Au/$Ni(OH)_2$ (Light)	-	270	GCE	5
Au/$Ni(OH)_2$ (Dark)	1.47	330	GCE	5
LiNiCo-OH	1.52	340	GCE	6
$FeCoNiO_x$	1.42	-	GCE	7
$NiCo_{2.7}OH$	1.48	350	GCE	8
NiCo LDH/CP	1.53	367	Carbon paper	9
$Ni_xCo_{3-x}O_4$ nanowie array/Ti foil	-	370	Ti foil	10
$NiCo_2O_4$ nanowie Ti mesh	1.56	370	Ti mesh	11
NiFe-LDH NS	1.44	300	GCE	12
NiCoP/C	-	330	GCE	13
NiFe-MOFs array	-	240	GCE	14
$FeNiO_xH_y$	-	206	GCE	15
$NiCo_2O_4$	-	265	GCE	16
$Ni_{0.83}Fe_{0.17}(OH)_2$	-	245	GCE	17

References

1. S. Liu, X. Y. Guo, M. R. Li, W. H. Zhang, X. Y. Liu and C. Li, *Angew. Chem.-Int. Edit.*, 2011, **50**, 12050-12053.
2. J. Suntivich, K. J. May, H. A. Gasteiger, J. B. Goodenough and Y. Shao-Horn, *Science*, 2011, **334**, 1383-1385.
3. S. L. Zhao, Y. Wang, J. C. Dong, C. T. He, H. J. Yin, P. F. An, K. Zhao, X. F. Zhang, C. Gao, L. J. Zhang, J. W. Lv, J. X. Wang, J. Q. Zhang, A. M. Khattak, N. A. Khan, Z. X. Wei, J. Zhang, S. Q. Liu, H. J. Zhao and Z. Y. Tang, *Nat. Energy.*, 2016, **1**, 1-10.
4. G. T. Hai, X. L. Jia, K. Y. Zhang, X. Liu, Z. Y. Wu and G. Wang, *Nano Energy.*, 2018, **44**, 345-352.
5. G. G. Liu, P. Li, G. X. Zhao, X. Wang, J. T. Kong, H. M. Liu, H. B. Zhang, K. Chang, X. G. Meng, T. Kako and J. H. Ye, *J. Am. Chem. Soc.*, 2016, **138**, 9128-9136.
6. K. Y. Niu, F. Lin, S. Jung, L. Fang, D. Nordlund, C. C. L. McCrory, T. C. Weng, P. Ercius, M. M. Doeff and H. M. Zheng, *Nano Lett.*, 2015, **15**, 2498-2503.
7. R. D. L. Smith, M. S. Prevot, R. D. Fagan, Z. P. Zhang, P. A. Sedach, M. K. J. Siu, S. Trudel and C. P. Berlinguette, *Science.*, 2013, **340**, 60-63.
8. J. W. Nai, H. J. Yin, T. T. You, L. R. Zheng, J. Zhang, P. X. Wang, Z. Jin, Y. Tian, J. Z. Liu, Z. Y. Tang and L. Guo, *Adv. Energy Mater.*, 2015, **5**, 7.
9. H. F. Liang, F. Meng, M. Caban-Acevedo, L. S. Li, A. Forticaux, L. C. Xiu, Z. C. Wang and S. Jin, *Nano Lett.*, 2015, **15**, 1421-1427.
10. Y. G. Li, P. Hasin and Y. Y. Wu, *Adv. Mater.*, 2010, **22**, 1926-192.
11. Z. Peng, D. S. Jia, A. M. Al-Enizi, A. A. Elzatahry and G. F. Zheng, *Adv. Energy Mater.*, 2015, **5**, 7.
12. X. Y. Lu and C. A. Zhao, *Nat. Commun.*, 2015, **6**, 7.
13. P. He, X. Y. Yu and X. W. Lou, *Angew. Chem.-Int. Edit.*, 2017, **56**, 3897-3900.
14. J. J. Duan, S. Chen and C. Zhao, *Nat. Commun.*, 2017, **8**, 7.
15. X. J. Wu, Y. M. Zhao, T. Y. Xing, P. L. Zhang, F. S. Li, H. Lee, F. Li and L. C. Sun, *ChemSusChem*, 2018, **11**, 1761-1767.
16. Z. Chen, B. Zhao, Y. C. He, H. R. Wen, X. Z. Fu, R. Sun and C. P. Wong, *Mat. Chem. Front.*, 2018, **2**, 1155-1164.
17. Q. Zhou, Y. P. Chen, G. Q. Zhao, Y. Lin, Z. W. Yu, X. Xu, X. L. Wang, H. K. Liu, W. P. Sun and S. X. Dou, *ACS Catal.*, 2018, **8**, 5382-5390.